Composite Structures 330 (2024) 117821

Contents lists available at ScienceDirect

Composite Structures

journal homepage: www.elsevier.com/locate/compstruct

Design-oriented stress–strain model for RC columns with dual FRP- steel confinement mechanism

Javad Shayanfar [a,*], Joaquim A.O. Barros [a], Mohammadali Rezazadeh [b]

[a] ISISE, ARISE, Department of Civil Engineering, University of Minho, Azurém 4800-058, Guimarães, Portugal
[b] Department of Mechanical and Construction Engineering, Northumbria University, Newcastle upon Tyne NE1 8ST, United Kingdom

ARTICLE INFO

Keywords:
RC columns
Dual FRP and steel confinement
Stress–strain model
Design-oriented model

ABSTRACT

Many research studies have been conducted to evaluate confinement-induced enhancements on the mechanical properties of FRP (fiber-reinforced polymers)-confined plain concrete elements subjected to axial compressive loading, leading to the development of extensive predictive models. Nevertheless, experimental stress–strain results for FRP-confined RC columns (FCRC) have demonstrated some behavioural features that cannot be simulated accurately through this kind of model, developed exclusively for FRP-confined concrete columns (FCC). In this paper, a new design-oriented stress–strain model is proposed for the prediction of load-carrying capacity versus axial strain relationship of FCRC. For this purpose, a new parabolic stress–strain expression is developed for calculating the first branch of FCRC's response up to the transition zone, followed by a linear function. New formulations are proposed to determine the first branch's stress–strain gradient, transition zone-related information and the second branch's slope, calibrated using a large test database of FCRC. The proposed design-oriented model is capable of simulating accurately the combined influence of the dual FRP and steel confinement on load-carrying capacity versus axial strain relationship of FCRC. Lastly, the capability of this model is validated by comparison to existing experimental data of FCRC and those obtained from some of existing models in the literature.

1. Introduction

The usage of fiber-reinforced polymers (FRP) composites has become a well-established concept in engineering practice for retrofitting reinforced concrete (RC) elements. The full confinement of RC columns with externally bonded FRP jackets, as a competitive strengthening technique, has revealed a high potential to substantially improve their axial load-carrying capacity, deformability and energy dissipation [1–5]. Many research studies have been conducted to evaluate the beneficial influence of FRP confinement strategy on the mechanical properties of concrete columns subjected to axial compressive loading, leading to the development of many predictive models. Nevertheless, the applicability of most of these models is limited to FRP-confined concrete columns (FCC, as illustrated in Fig. 1). Consequently, these model do not consider the confinement provided by existing steel transverse reinforcements in the case of FRP-confined RC columns (FCRC, as illustrated in Fig. 1), neither the interaction of FRP and steel confining systems, recognized as a conservative assumption (Teng *et al.* [1]). As the confined concrete behavior under compression depends on the level of imposed confinement pressure, the consideration of dual FRP-steel confinement for an accurate simulation of the axial response of FCRC can be of significant interest, as the main objective of the present study.

For a thorough examination of available research studies in the literature, they were presented into the following groups: Group A) those performing axial compressive tests on FCRC for the evaluation of the performance of dual FRP-steel confinement on enhancing axial and dilation behavior of RC columns; Group B) those with a theoretical framework that analytically formulate the axial stress–strain response of FCRC columns.

In the Group A, Wang *et al.* [2] experimentally evidenced that the combined FRP-steel confinement in case of FCRC leads to considerable improvements in terms of axial response in comparison with those induced solely by FRP confinement in case of FCC. Based on the dilation responses of FCRC and FCC specimens with similar FRP confinement stiffness conducted by Barros and Ferreira [3], concrete in FCRC has a shorter volumetric expansion with a lower dilatancy compared to that in

* Corresponding author.
E-mail addresses: id8287@alunos.uminho.pt (J. Shayanfar), barros@civil.uminho.pt (J.A.O. Barros), mohammadali.rezazadeh@northumbria.ac.uk (M. Rezazadeh).

https://doi.org/10.1016/j.compstruct.2023.117821
Received 24 July 2023; Received in revised form 24 November 2023; Accepted 15 December 2023
Available online 19 December 2023

FCC, which can be attributed to the capability of the FRP-steel confinement in counteracting the concrete tendency for stiffness degradation (Shayanfar *et al.* [4]). Eid *et al.* [5] evidenced that increasing volumetric steel reinforcement ratio postpones FRP rupture in FCRC, caused by the curtailment in concrete dilation, resulting in an increase in peak strength and deformability. The experimental study conducted by Kaeseberg *et al.* [6] revealed the effectiveness of FRP-steel confinement is more pronounced in the case of steel spiral compared to steel hoops. Wei *et al.* [7] experimentally demonstrated that the level of enhancements offered by FRP-steel confinement is strongly dependent on steel hoop spacing, as also verified by Lee *et al.* [8] and Yin *et al.* [9]. Benzaid *et al.* [10] experimentally evidenced that by increasing concrete strength, the effectiveness of the FRP-steel confinement in axial and dilation responses of FCRC tends to reduce noticeably, as also evidenced by Issa *et al.* [11]. By using finite element analysis, Zignago and Barbato [12] revealed that the contribution of steel confinement on load-carrying capacity of FCRC reduces by increasing FRP confinement stiffness and concrete strength. Carey and Harries [13] conducted axial compressive tests on small-, medium-, and large-scale FCRC columns to identify scale effects in their axial behavior. The results revealed that the column scale does not have a significant influence on the normalized axial stress–strain response. Ilki *et al.* [14] verified experimentally that providing a sufficient level of FRP confinement imposed to the cover concrete is able to prevent the spalling mechanism, and also can maintain the FRP-steel dual confinement until very large axial deformations. Bai *et al.* [15] investigated the effect of FRP confinement on the buckling of steel longitudinal bars in FCRC columns. It was found that the FRP confinement is capable of restraining the longitudinal reinforcements against buckling, so that this phenomenon is much more likely in FCRC with largely-spaced steel hoops, lightly confined by FRP jacket, resulting in a reduction in the column deformability.

In the Group B, several analytical models have been proposed to predict the stress–strain response of FCRC columns, which can be categorized into two groups: i) analysis-oriented models (AOM); ii) design-oriented models (DOM). AOM are founded on equilibrium conditions and radial displacement compatibility between FRP confinement pressure and the confined concrete based on an incremental approach, whose calculation process has two main steps. First, by using a dilation model, the relationship of FRP hoop strain, generating a specific confinement pressure, with axial strain is obtained. Then, at a specific axial strain, the corresponding axial stress is determined through an axial stress-axial strain base relation (developed for actively-confined concrete), where the difference of passive confinement (i.e. FRP) with active one is reflected in the peak point of this base relation (generally known as failure surface function). Accordingly, the reliability of a AOM depends not only on the accuracy of its failure surface function, but also on that of the coupled dilation model, which may not return close prediction of the complete axial stress–strain response of FCRC. Hu and Seracino [16] developed AOM for predicting stress–strain relation of FCRC based on Jiang and Teng [17]'s AOM developed exclusively for FCC. In this model, the contribution of FRP jacket and steel transverse reinforcements in the dilation model was reflected based on experimental observations. Furthermore, the effect of steel transverse reinforcements in failure surface function was considered using Mander *et al.* [18]'s recommendation, suggested exclusively for RC columns (steel confined concrete - SCC). Likewise, Teng *et al.* [1] extended Jiang and Teng [17]'s AOM for FCRC. In this model, the effect of dual FRP-steel confinement mechanism in terms of dilation model and failure surface function is implemented by introducing a FRP-steel stiffness parameter as the ratio of the confinement stiffness of FRP jacket and steel transverse reinforcements. Shayanfar *et al.* [19] proposed an AOM for FCRC with either FRP full or partial confinement arrangement. In this model, Teng *et al.* [1]'s dilation model developed for FCRC was improved through the consideration of the influence of non-homogenous distribution of concrete lateral expansion along the column height. Furthermore, the failure surface function suggested by Shayanfar *et al.* [20], developed exclusively for FCC, was extended for FCRC by considering the influence of steel transverse reinforcements.

Regarding DOM, they provide a simpler calculation format, where closed-form formulations, developed based on the shape of the axial stress–strain curve, are used, whose key coordinates (i.e. transition and ultimate stages) are calibrated through relevant experimental data. Eid and Paultre [21] proposed a two-segment DOM for predicting stress–-strain relation of FCRC based on the Légeron and Paultre [22]'s model developed for SCC. In this model, FCRC's response was related to a FRP-steel confinement index considering the mechanical and geometric properties of the concrete, FRP jacket and steel transverse reinforcement. Pellegrino and Modena [23] proposed a two-segment DOM, by deriving from experimental results the strain/stress data defining the transition and ultimate points of the model. Wang *et al.* [2] developed a single-segment DOM for FCRC, where the peak strength and the corresponding axial strain in stress–strain relation of FCRC were calibrated based on test data. However, the model considered an average level of axial stress–strain responses for both concrete cover and core regions, which can affect detrimentally its predictive performance. Lin *et al.* [24] proposed a three-segment DOM for FCRC, where the transition stress and strain, and the slope of the stress–strain hardening branch were determined/calibrated by performing regression analysis with numerical data obtained from Teng *et al.* [1]'s AOM developed for FCRC.

It is noteworthy that the stress–strain relationships of FCRC developed by DOM were built unavoidably through regression analysis implemented in a set of test data of FCRC. Hence, the reliability and

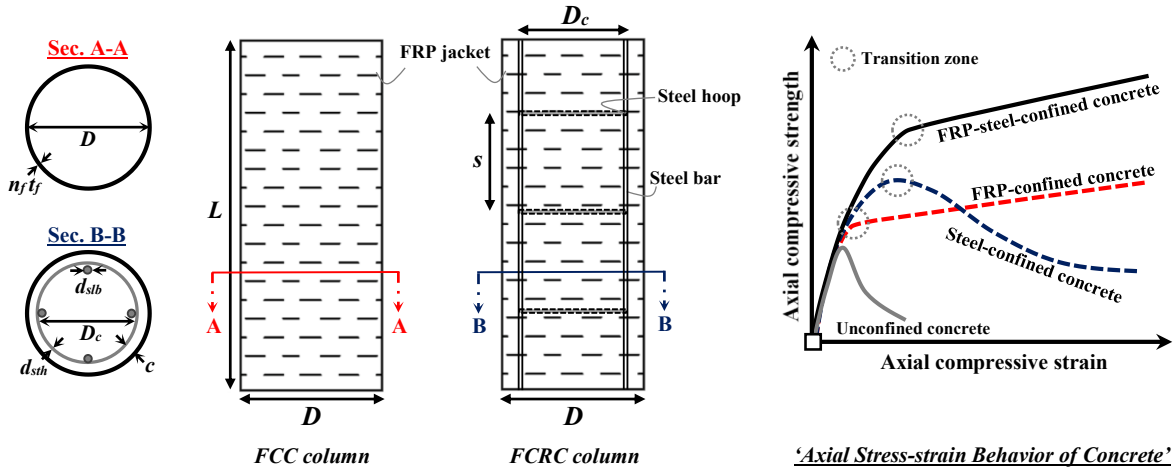

Fig. 1. Circular concrete/RC columns fully confined with FRP jacket.

applicability of these models is limited to the extensiveness and range of main variables involved in the adopted database. Since existing DOMs were generally founded based on a limited test data of FCRC available at the time of their research study, these models can be recalibrated with expectable improvements in its reliability and applicability. This also justifies the consideration of a continuous process of the data collection for the database, and subsequently the recalibration of DOM.

This paper is dedicated to the establishment of a new DOM, formed by two branches, for the prediction of load-carrying capacity versus axial strain relationship of FCRC subjected to axial compressive loading. For this purpose, a new parabolic stress–strain expression is proposed for calculating the first branch of FCRC's response up to the transition zone. The stress–strain gradient of the proposed function was calibrated using a large test database of FCRC, FCC and unconfined concrete specimens. Subsequently, new formulations, with a unified character for SCC, are developed to determine the transition zone-related information, calibrated based on a large database of FCRC. A linear function is considered for the second branch of axial stress–strain curve, whose slope is derived based on a new methodology. In the proposed model, the cover concrete region (subjected to only FRP confinement) and the core concrete one (subjected to a combined FRP-steel confinement) are treated separately. With these features, the proposed DOM can objectively account for the integrated influence of dual FRP and steel confinement on load-carrying capacity versus axial strain relationship of FCRC. Lastly, the capability of this model is validated by comparison to existing experimental data of FCRC and those obtained from some of existing DOMs and AOMs recommended by Wang *et al.* [2], Hu and Seracino [16], Teng *et al.* [1], Lin *et al.* [24], ACI440.2R-17 [25] and *fib* [26].

2. Load-carrying capacity versus axial strain relationship

In this section, the load-carrying capacity (N) versus axial strain (ε_c) relationship for FCRC under axial compressive loading is determined. Under such loading conditions, as illustrated in Fig. 2, three distinct components of FCRC carry compressive loads including: i) concrete cover, ii) concrete core, and iii) longitudinal steel bars. In this approach, a uniform axial strain distribution is assumed acting on the entire cross-section and also along the column height.

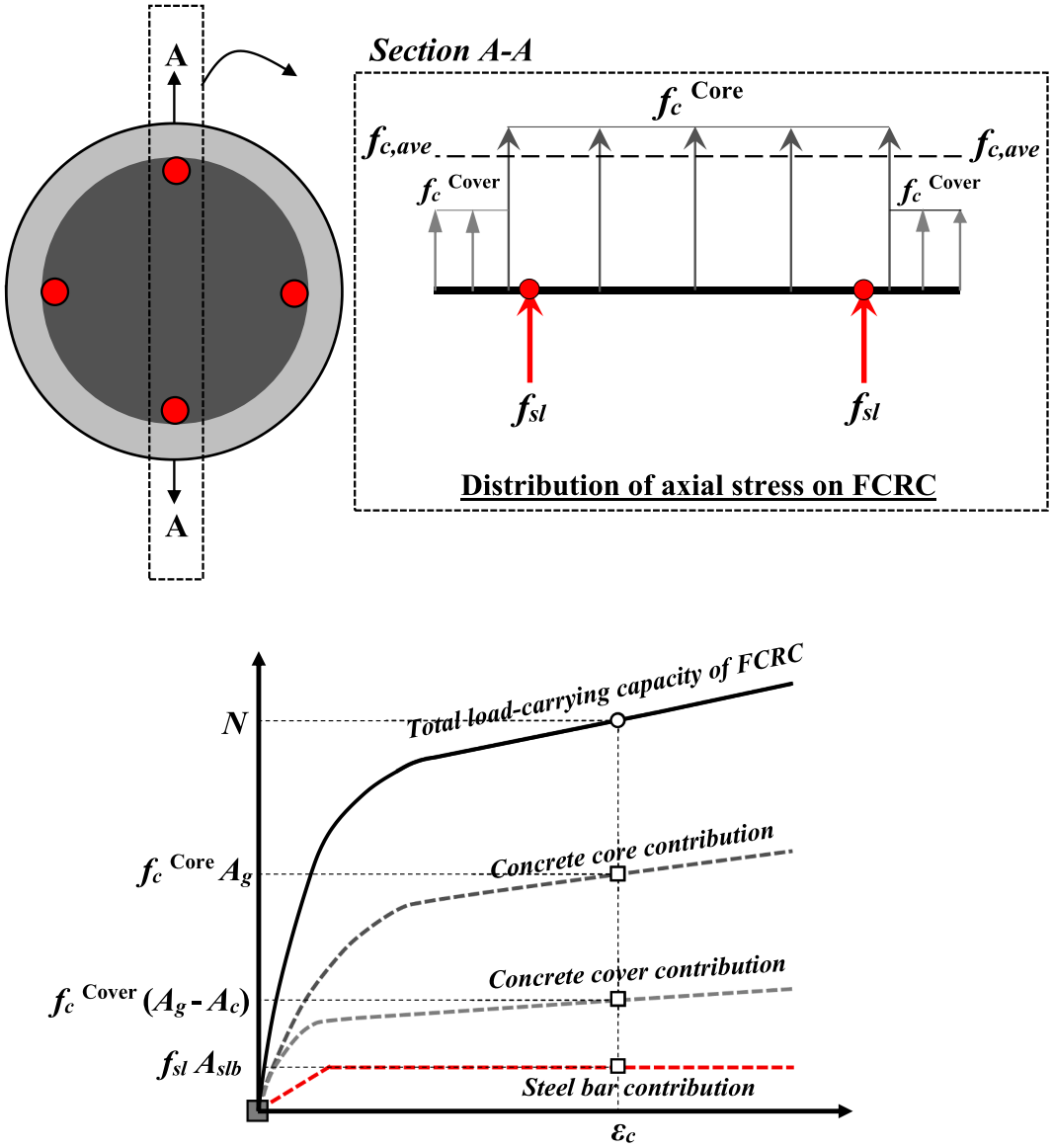

Fig. 2. Distinct load-carrying parts of FCRC.

Accordingly, N at a specific ε_c can be calculated as the summation of the load-carrying capacity from these components:

$$N = f_{c,ave}A_g + f_{sl}A_{slb} \tag{1}$$

in which

$$f_{c,ave} = f_c^{Core}\frac{A_c}{A_g} + f_c^{Cover}\left(1 - \frac{A_c}{A_g}\right) \tag{2}$$

$$f_{sl} = E_{sl}\varepsilon_c \leqslant f_{yl} \tag{3}$$

where $f_{c,ave}$ is the axial stress carried by concrete acting on the entire cross-section with the area of A_g; f_c^{Core} is the axial stress acting on the concrete core with the area of $A_c = \pi D_c^2/4$; f_c^{Cover} is the axial stress acting on the concrete cover with the area of $A_g - A_c = \pi(D - D_c)^2/4$; f_{sl} is the axial stress carried by steel longitudinal bars with the area of A_{slb}; E_{sl} and f_{yl} are the elasticity modulus and yield stress of steel longitudinal bars, respectively.

It is noteworthy that column elements are never subjected to purely axial loads. Therefore, under operational procedures, the concrete cover plays a significant role in the overall behavior, particularly under reversed cyclic loading [27–29]. It is one of the reasons that FRP continuous-sheets are appealing as a retrofit of existing confinement-deficient columns. Accordingly, ignoring the important difference between the cover concrete (subjected to only FRP confinement) and the core concrete (subjected to a combined FRP-steel confinement) can be considered as a significant disadvantage for a stress–strain model of FCRC. Rather, treating these parts separately in a stress–strain model of FCRC could be a more realistic solution and more favourable for a moment–curvature analysis, which is typically used for analysing FCRC under seismic loading (combined axial load and flexure). Accordingly, in the present study, different stress–strain relationships were treated for the cover concrete (f_c^{Cover} *vs* ε_c) and the core concrete (f_c^{Core} *vs* ε_c).

3. Determination of f_c^{Cover} and f_c^{Core} versus ε_c relationships

In this study, based on experimental observations (i.e. [5–9]), a model is proposed for defining a stress–strain relationship composed by two branches for both concrete core and cover parts. The first branch is formed by a parabolic equation up to the transition phase, and the second by a linear relationship. Accordingly, for the concrete cover of FCRC, on the basis of the stress–strain behavior of FCC, a formulation containing two stress–strain branches is suggested for f_c^{Cover} versus ε_c relationship as (Fig. 3):

$$f_c^{Cover} = \left[A_1^F\left(\frac{\varepsilon_c}{\varepsilon_{ctr}^F}\right)^{n_d} + A_2^F\left(\frac{\varepsilon_c}{\varepsilon_{ctr}^F}\right)\right]f_{ctr}^F \quad for \quad \varepsilon_c \leqslant \varepsilon_{ctr}^F \tag{4a}$$

$$f_c^{Cover} = f_{ctr}^F + E_2^F\left(\varepsilon_c - \varepsilon_{ctr}^F\right) \quad for \quad \varepsilon_c \geqslant \varepsilon_{ctr}^F \tag{4b}$$

in which

$$A_1^F = \frac{1 - E_2^F/E_{ctr}^F}{1 - n_d} \tag{5}$$

$$A_2^F = \frac{E_2^F}{E_{ctr}^F} - \frac{n_d}{1 - n_d}\left(1 - \frac{E_2^F}{E_{ctr}^F}\right) \tag{6}$$

$$E_{ctr}^F = \frac{f_{ctr}^F}{\varepsilon_{ctr}^F} \tag{7}$$

where the "F" in the subscript represents the FRP confinement imposed to the concrete cover; A_1^F and A_2^F are the coefficients of the polynomial function that are determined based on the boundary conditions as i) $f_c^{Cover}\left(\varepsilon_c = \varepsilon_{ctr}^F\right) = f_{ctr}^F$ and ii) $\left(df_c^{Cover}/d\varepsilon_c\right)_{\varepsilon_c = \varepsilon_{ctr}^F} = E_2^F$; f_{ctr}^F and ε_{ctr}^F are the axial stress and its corresponding axial strain of the concrete cover's behavior at the transition zone; n_d is the degree of the polynomial function, adjusting the rate of the change of the first branch of f_c^{Cover} versus ε_c relationship (to be presented in the next section); E_2^F is the slope of the second branch.

For the establishment of the axial stress–strain relationship of the concrete core subjected to a dual FRP-steel confinement mechanism, an approach similar to the one adopted in the concrete cover was followed, namely (Fig. 3):

$$f_c^{Core} = \left[A_1^{FS}\left(\frac{\varepsilon_c}{\varepsilon_{ctr}^{FS}}\right)^{n_d} + A_2^{FS}\left(\frac{\varepsilon_c}{\varepsilon_{ctr}^{FS}}\right)\right]f_{ctr}^{FS} \quad for \quad \varepsilon_c \leqslant \varepsilon_{ctr}^{FS} \tag{8a}$$

$$f_c^{Core} = f_{ctr}^{FS} + E_2^{FS}\left(\varepsilon_c - \varepsilon_{ctr}^{FS}\right) \quad for \quad \varepsilon_c \geqslant \varepsilon_{ctr}^{FS} \tag{8b}$$

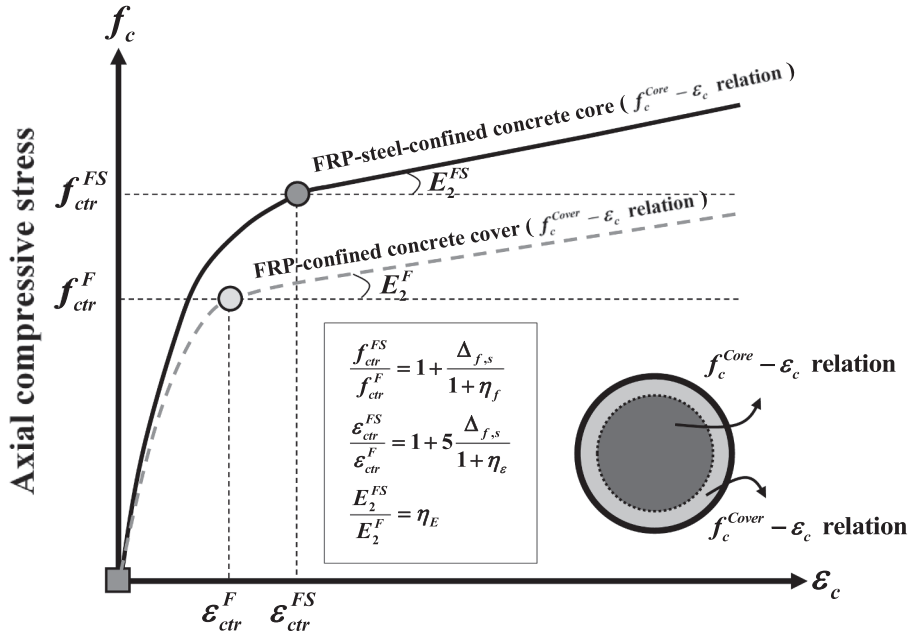

Fig. 3. Physical representation of f_c^{Cover} and f_c^{Core} versus ε_c relationships.

in which

$$A_1^{FS} = \frac{1 - E_2^{FS}/E_{ctr}^{FS}}{1 - n_d} \tag{9}$$

$$A_2^{FS} = \frac{E_2^{FS}}{E_{ctr}^{FS}} - \frac{n_d}{1 - n_d}\left(1 - \frac{E_2^{FS}}{E_{ctr}^{FS}}\right) \tag{10}$$

$$E_{ctr}^{FS} = \frac{f_{ctr}^{FS}}{\varepsilon_{ctr}^{FS}} \tag{11}$$

where the "FS" in the subscript represents the FRP-steel confinement imposed to the concrete core; A_1^{FS} and A_2^{FS} are the coefficients of the polynomial function that are determined based on the boundary conditions as i) $f_c^{Core}\left(\varepsilon_c = \varepsilon_{ctr}^{FS}\right) = f_{ctr}^{FS}$ and ii) $\left(df_c^{Core}/d\varepsilon_c\right)_{\varepsilon_c = \varepsilon_{ctr}^{FS}} = E_2^{FS}$; f_{ctr}^{FS} and ε_{ctr}^{FS} are the axial stress and its corresponding axial strain of the concrete cover at the transition zone; n_d is the degree of the polynomial function, adjusting the rate of the change of the first branch of f_c^{Core} versus ε_c relationship (to be presented in next section); E_2^{FS} is the slope of the second branch.

To calculate f_c^{Cover} and f_c^{Core} versus ε_c relationships by Eqs. (4) and (8), respectively, the transition zone-related information (f_{ctr}^{F} and ε_{ctr}^{F}, f_{ctr}^{FS}, ε_{ctr}^{FS},) and the slopes of the second branches (E_2^F and E_2^{FS}) are required to be determined as input parameters, which is presented in the following sections.

4. Database of axial compressive tests on FCRC

In the current study, a large database, including 97 test specimens from existing axial compressive tests performed on FCRC, was collected for the development and assessment of predictive models. These tests were conducted by Demers and Neale [30], Pessiki *et al.* [31], Matthys *et al.* [32], Barros and Ferreira [3], Eid *et al.* [5], Lee *et al.* [8], Chastre and Silva [33], Wang *et al.* [2], Zhang [34], Wei *et al.* [7], Kaeseberg *et al.* [6] and Wei *et al.* [35], and the relevant information is presented in Table 1. In all FCRC specimens, fibers of FRP confining system were oriented in the hoop direction, and specimens with helical wrapping arrangements are not part of the database. Furthermore, tests with incomplete data for defining the axial stress versus axial strain curves are also not considered.

The majority of the test specimens collected in the database are relatively large-scale FCRC specimens. It is well-known that the compressive strength of unconfined concrete (f_{c0}) is size-dependent, so the f_{c0} is noticeably lower than the corresponding compressive strength in standard concrete cylinder of 150 × 300 mm ($f_{c0}^{'}$). Therefore, for test programs with f_{c0} not available, the formulation recommended by Sim *et al.* [36] was used to obtain f_{c0} from $f_{c0}^{'}$ as follows:

$$f_{c0} = 1.063\left(\frac{150}{D}\right)^{0.122}\left(\frac{D}{L}\right)^{0.088} f_{c0}^{'} \tag{12}$$

where D and L is, respectively, the dimeter and the height of the column. Moreover, in the present study, to calculate the axial strain (ε_{c0}) corresponding to f_{c0}, Shayanfar *et al.* [37]'s formulation considering size effect was adopted:

$$\varepsilon_{c0} = 0.0011\left(\frac{f_{c0}D}{L}\right)^{0.25} \tag{13}$$

It is noteworthy that steel longitudinal rebars might experience buckling mechanism during axial compressive loading, particularly in RC columns with largely-spaced steel hoops since it decreases the resistance of stirrups' concrete cover to the buckling of this reinforcement. Nonetheless, FRP confinement is able to restrain the compressed rebars to buckling mechanism, depending on the stiffness of the FRP-cover-stirrups system ([15]). Wang *et al.* [2] experimentally evidenced that until the fracture of steel hoops or the rupture of FRP confining system, the buckling of steel longitudinal rebars in FCRC columns with sufficient confinement stiffness does not occur. Bai *et al.* [15] experimentally demonstrated that for the case of FCRC with largely-spaced steel hoops of $R_s = s/D_c = 2.5$ (where D_c is the dimeter of concrete core), the buckling of steel longitudinal bars occurred prior to the FRP rupture stage, leading to a premature failure of FRP rupture, which was also confirmed by Zhang [34]. Furthermore, the buckling of compressed bars might result in a reduction in FRP-steel confinement pressure, due to the contribution of FRP-steel lateral pressure in restraining the bars' buckling. Consequently, a reduction in FRP-steel confinement-induced improvements in terms of ductility and load-carrying capacity is expected. Based on aforementioned discussion, in the present study, to have a consistent database, FCRC specimens with R_s higher than 1.3 are not considered. Since in FCRC with $R_s \leqslant 1.3$, the effect of buckling of steel longitudinal bars tends to be marginal, the present study does not take into account the buckling's effect, assuming a relatively adequate reciprocal lateral stiffness of FRP-cover-stirrups imposed to longitudinal rebars in the specimens collected in the database.

5. Determination of transition zone-related information

In order to calculate f_{ctr}^{F} and ε_{ctr}^{F} related to the concrete cover subjected to only FRP confinement, in this study, the well-calibrated formulations recommended by Shayanfar *et al.* [38] and [39] developed exclusively for FCC was adopted. Accordingly, based on this recommendation, the transition zone-related information can be calculated by:

$$\frac{f_{ctr}^{F}}{f_{c0}} = 1 + 0.043\left(\frac{K_{Lf}}{f_{c0}}\right)^{0.4} \tag{14}$$

$$\frac{\varepsilon_{ctr}^{F}}{\varepsilon_{c0}} = 0.45\psi_K f_{c0}^{0.25} + 0.0075K_{Lf}^{0.37} \geqslant 1 \tag{15}$$

in which

$$\psi_K = 0.7K_{Lf}^{0.07} \leqslant 1 \tag{16}$$

$$K_{Lf} = 2\frac{n_f t_f E_f}{D} \tag{17}$$

where K_{Lf} is the FRP lateral confinement stiffness; n_f is the number of FRP layers; t_f is the nominal thickness of a FRP layer; E_f is the FRP modulus elasticity. However, the transition zone of the concrete core's stress–strain relation of FCRC is not only dependent on FRP confinement, but also of the steel confinement and their interactions. Thus, the increase of the values of these variables (f_{ctr}^{FS} and ε_{ctr}^{FS}) compared to those associated to unconfined concrete (f_{c0} and ε_{c0}) is a main function of FRP-steel confinement-induced improvements. It should be noted that SCC columns can be considered a special case of FCRC when FRP confinement stiffness (K_{Lf}) approaches to zero. In this special case of SCC, the transition phase can be defined at its peak stage. Mander *et al.* [18] proposed a well-established formulation to determine the peak stage of SCC, which has been extensively being adopted in the literature. By adopting Mander *et al.* [18]'s recommendations, the steel-induced improvements ($\Delta_{f,s}$) in terms of peak axial strength (f_{cc}^{S}) can be calculated by:

$$\frac{f_{cc}^{S}}{f_{c0}} = 1 + \Delta_{f,s} \tag{18}$$

in which

$$\Delta_{f,s} = 2.254\sqrt{1 + 7.94\frac{f_{ls,y}}{f_{c0}}} - 2\frac{f_{ls,y}}{f_{c0}} - 2.254 \tag{19}$$

Table 1
Details of the complied dataset of FCRC specimens.

Reference ID	D (mm)	L (mm)	C (mm)	f_{c0} (MPa)	ε_{c0} (MPa)	n_f	t_f (mm)	E_f (GPa)	ε_{fu}	n_{slb}	d_{slb} (mm)	f_{yl} (MPa)	d_{sth} (mm)	S (mm)	f_{yh} (MPa)	Steel type	
Demers and Neale [30]	U25-1	300	1200	22	24.9	0.0017	3	0.300	84	0.015	5	11.3	400	6.4	300	400	H
	U25-2	300	1200	19	24.9	0.0017	3	0.300	84	0.015	5	16	400	11.3	150	400	H
	U25-3	300	1200	22	24.9	0.0017	3	0.300	84	0.015	5	19.5	400	6.4	150	400	H
	U25-4	300	1200	19	24.9	0.0017	3	0.300	84	0.015	5	25.2	400	11.3	300	400	H
Pessiki et al. [31]	C3	508	1830	29	26.8	0.0018	3	1.000	21.8	0.019	8	22	457	9.5	356	502	H
	C4	508	1830	29	26.8	0.0018	3	1.000	38.1	0.015	8	22	457	9.5	356	502	H
Matthys et al. [32]	K2	400	2000	15	31.8	0.0017	5	0.117	198	0.012	10	12	620	8	140	560	H
	K3	400	2000	15	31.8	0.0017	4	0.235	480	0.002	10	12	620	8	140	560	H
	K4	400	2000	15	31.8	0.0017	6	0.300	60	0.013	10	12	620	8	140	560	H
	K8	400	2000	15	31.8	0.0017	4	0.123	120	0.010	10	12	620	8	140	560	H
Barros and Ferreira [3]	L3S200C16	200	600	20	12.9	0.0016	3	0.113	232	0.015	4	10	421	6	120	468	H
	L5S200C16	200	600	20	12.9	0.0016	3	0.176	230	0.015	4	10	421	6	120	468	H
	L3S300C16	200	600	20	12.9	0.0016	5	0.113	232	0.015	4	10	421	6	120	468	H
	L5S300C16	200	600	20	12.9	0.0016	5	0.176	230	0.015	4	10	421	6	120	468	H
	L3S200C32	200	600	20	28.2	0.0019	3	0.113	232	0.015	4	10	421	6	120	468	H
	L5S200C32	200	600	20	28.2	0.0019	3	0.176	230	0.015	4	10	421	6	120	468	H
	L3S300C32	200	600	20	28.2	0.0019	5	0.113	232	0.015	4	10	421	6	120	468	H
	L5S300C32	200	600	20	28.2	0.0019	5	0.176	230	0.015	4	10	421	6	120	468	H
Lee et al. [8]	S6F1	150	300	7.5	36.2	0.0023	1	0.110	250	0.018	–	–	–	5	60	1200	S
	S6F2	150	300	7.5	36.2	0.0023	2	0.110	250	0.018	–	–	–	5	60	1200	S
	S6F3	150	300	7.5	36.2	0.0023	3	0.110	250	0.018	–	–	–	5	60	1200	S
	S6F4	150	300	7.5	36.2	0.0023	4	0.110	250	0.018	–	–	–	5	60	1200	S
	S6F5	150	300	7.5	36.2	0.0023	5	0.110	250	0.018	–	–	–	5	60	1200	S
	S4F1	150	300	7.5	36.2	0.0023	1	0.110	250	0.018	–	–	–	5	40	1200	S
	S4F2	150	300	7.5	36.2	0.0023	2	0.110	250	0.018	–	–	–	5	40	1200	S
	S4F3	150	300	7.5	36.2	0.0023	3	0.110	250	0.018	–	–	–	5	40	1200	S
	S4F4	150	300	7.5	36.2	0.0023	4	0.110	250	0.018	–	–	–	5	40	1200	S
	S4F5	150	300	7.5	36.2	0.0023	5	0.110	250	0.018	–	–	–	5	40	1200	S
	S2F1	150	300	7.5	36.2	0.0023	1	0.110	250	0.018	–	–	–	5	20	1200	S
	S2F2	150	300	7.5	36.2	0.0023	2	0.110	250	0.018	–	–	–	5	20	1200	S
	S2F3	150	300	7.5	36.2	0.0023	3	0.110	250	0.018	–	–	–	5	20	1200	S
	S2F4	150	300	7.5	36.2	0.0023	4	0.110	250	0.018	–	–	–	5	20	1200	S
	S2F5	150	300	7.5	36.2	0.0023	5	0.110	250	0.018	–	–	–	5	20	1200	S
Eid et al. [5]	A5NP2C	303	1200	25	25.4	0.0018	2	0.381	78	0.013	6	16	423	9.5	150	602	H
	A3NP2C	303	1200	25	27.4	0.0018	2	0.381	78	0.013	6	16	550	9.5	70	602	H
	A1NP2C	303	1200	25	27.4	0.0018	2	0.381	78	0.013	6	16	487	9.5	45	602	H
	B4NP2C	303	1200	25	27.4	0.0018	2	0.381	78	0.013	6	16	550	11.3	100	456	H
	C4NP2C	303	1200	25	27.4	0.0018	2	0.381	78	0.013	6	16	423	11.3	100	456	S
	C4N1P2C	303	1200	25	31.1	0.0018	2	0.381	78	0.013	6	16	423	11.3	100	456	S
	C4NP4C	303	1200	25	27.4	0.0018	4	0.381	78	0.013	6	16	423	11.3	100	456	S
	C4MP2C	303	1200	25	43.9	0.0020	2	0.381	78	0.013	6	16	423	11.3	100	456	S
	C2NP2C	303	1200	25	27.4	0.0018	2	0.381	78	0.013	6	16	423	11.3	65	456	S
	C2N1P2C	303	1200	25	31.1	0.0018	2	0.381	78	0.013	6	16	423	11.3	65	456	S
	C2N1P4C	303	1200	25	31.1	0.0018	4	0.381	78	0.013	6	16	423	11.3	65	456	S
	C2N1P2N	253	1200	0	31.3	0.0018	2	0.381	78	0.013	6	16	423	11.3	65	456	S
	C2MP2C	303	1200	25	43.9	0.0020	2	0.381	78	0.013	6	16	424	11.3	65	456	S
	C2MP4C	303	1200	25	43.9	0.0020	4	0.381	78	0.013	6	16	425	11.3	65	456	S
	C2MP2N	253	1200	0	44.2	0.0019	2	0.381	78	0.013	6	16	426	11.3	65	456	S
Chastre and Silva [33]	C10	150	750	15	38.0	0.0018	2	0.167	226	0.014	6	6	391	3	100	323	H
	C11	150	750	15	38.0	0.0018	2	0.167	226	0.014	6	6	391	3	100	323	H
	C15	150	750	15	38.0	0.0018	2	0.167	226	0.014	6	6	391	3	150	323	H
	C19	150	750	15	38.0	0.0018	2	0.167	226	0.014	6	6	391	3	50	323	H
	C41	250	750	25	34.9	0.0020	1	0.176	241	0.015	6	12	458	6	150	391	H
	C34	250	750	25	34.9	0.0020	2	0.176	241	0.015	6	12	458	6	150	391	H

(*continued on next page*)

Table 1 (*continued*)

Reference ID	D (mm)	L (mm)	C (mm)	f_{c0} (MPa)	ε_{c0} (MPa)	n_f	t_f (mm)	E_f (GPa)	ε_{fu}	n_{slb}	d_{slb} (mm)	f_{yl} (MPa)	d_{sth} (mm)	S (mm)	f_{yh} (MPa)	Steel type	
	C43	250	750	25	34.9	0.0020	3	0.176	241	0.015	6	12	458	6	150	391	H
	C44	250	750	25	34.9	0.0020	4	0.176	241	0.015	6	12	458	6	150	391	H
Wang et al. [2]	C1H1L1M	305	915	18	21.7	0.0018	1	0.167	244	0.018	8	12	340	6	80	397	H
	C1H1L1C	305	915	18	21.7	0.0018	1	0.167	244	0.018	8	12	340	6	80	397	H
	C1H1L2M	305	915	18	21.7	0.0018	2	0.167	244	0.018	8	12	340	6	80	397	H
	C1H1L2C	305	915	18	21.7	0.0018	2	0.167	244	0.018	8	12	340	6	80	397	H
	C1H2L1M	305	915	18	21.7	0.0018	1	0.167	244	0.018	8	12	340	6	40	397	H
	C1H2L2M	305	915	18	21.7	0.0018	2	0.167	244	0.018	8	12	340	6	40	397	H
	C2H1L1M	204	612	12	22.8	0.0018	1	0.167	244	0.018	6	10	312	6	120	397	H
	C2H1L1C	204	612	12	22.8	0.0018	1	0.167	244	0.018	6	10	312	6	120	397	H
	C2H1L2M	204	612	12	22.8	0.0018	2	0.167	244	0.018	6	10	312	6	120	397	H
	C2H1L2C	204	612	12	22.8	0.0018	2	0.167	244	0.018	6	10	312	6	120	397	H
	C2H2L1M	204	612	12	22.8	0.0018	1	0.167	244	0.018	6	10	312	6	60	397	H
	C2H2L1C	204	612	12	22.8	0.0018	1	0.167	244	0.018	6	10	312	6	60	397	H
	C2H2L2M	204	612	12	22.8	0.0018	2	0.167	244	0.018	6	10	312	6	60	397	H
	C2H2L2C	204	612	12	22.8	0.0018	2	0.167	244	0.018	6	10	312	6	60	397	H
Zhang [34]	CF1T300	350	1300	40	21.4	0.0017	2	0.171	242	0.016	6	20	495	8	300	430	H
	CF0.5 T300	350	1300	40	28.2	0.0018	1	0.171	242	0.016	6	20	497	8	300	430	H
	CF1T90	350	1300	40	39.3	0.0020	2	0.171	242	0.016	6	20	511	8	90	358	H
	CF1T150	350	1300	40	39.3	0.0020	2	0.171	242	0.016	6	20	511	8	150	358	H
	CF1.5 T150	350	1300	40	39.3	0.0020	3	0.171	242	0.016	6	20	511	8	150	358	H
Wei et al. [7]	CS20B1	150	300	5	40.2	0.0023	1	0.167	74.1	0.022	–	–	–	6	20	365	S
	CS40B1	150	300	5	40.2	0.0023	1	0.167	74.1	0.022	–	–	–	6	40	365	S
	CS60B1	150	300	5	40.2	0.0023	1	0.167	74.1	0.022	–	–	–	6	60	365	S
	CS20B2	150	300	5	40.2	0.0023	2	0.167	74.1	0.022	–	–	–	6	20	365	S
	CS40B2	150	300	5	40.2	0.0023	2	0.167	74.1	0.022	–	–	–	6	40	365	S
	CS60B2	150	300	5	40.2	0.0023	2	0.167	74.1	0.022	–	–	–	6	60	365	S
	CS20C1	150	300	5	40.2	0.0023	1	0.167	249.8	0.017	–	–	–	6	20	365	S
	CS40C1	150	300	5	40.2	0.0023	1	0.167	249.8	0.017	–	–	–	6	40	365	S
	CS60C1	150	300	5	40.2	0.0023	1	0.167	249.8	0.017	–	–	–	6	60	365	S
	CS20C2	150	300	5	40.2	0.0023	2	0.167	249.8	0.017	–	–	–	6	20	365	S
	CS40C2	150	300	5	40.2	0.0023	2	0.167	249.8	0.017	–	–	–	6	40	365	S
	CS60C2	150	300	5	40.2	0.0023	2	0.167	249.8	0.017	–	–	–	6	60	365	S
Kaeseberg et al. [6]	D20-TR-M2-2L-3a	200	400	15	27.0	0.0021	2	0.111	230	0.018	4	12	500	6	100	550	H
	D20-TR-M2-2L-3b	200	400	15	27.0	0.0021	2	0.111	230	0.018	6	12	500	6	100	550	H
	D20-TR-M2-2L-3c	200	400	15	27.0	0.0021	2	0.111	230	0.018	8	12	500	6	100	550	H
	D25-SR-M1-2L-3	250	1000	15	27.6	0.0018	2	0.111	230	0.017	6	12	500	8	40	550	S
	D25-TR-M1-2L-2	250	1000	15	27.6	0.0018	2	0.111	230	0.017	6	12	500	6	100	550	H
	D30-SR-M1-2L-2	300	600	15	28.5	0.0021	2	0.111	230	0.017	6	12	500	10	55	550	S
Wei et al. [35]	SR75S20B1	150	300	0	40.2	0.0023	1	0.167	74.1	0.022	–	–	–	8	20	326	S
	SR75S20B2	150	300	0	40.2	0.0023	2	0.167	74.1	0.022	–	–	–	8	20	326	S
	SR75S20C1	150	300	0	29.4	0.0022	1	0.167	250	0.017	–	–	–	8	20	326	S
	SR75S20C2	150	300	0	29.4	0.0022	2	0.167	250	0.017	–	–	–	8	20	326	S

Note: D = the diameter of the column; L = the column height; c = the thickness of the concrete cover; f_{c0} = the compressive strength of unconfined concrete considering size effect; ε_{c0} = the axial strain corresponding to f_{c0}; n_f = the number of FRP layer; t_f = the nominal thickness of a FRP layer; E_f = FRP modulus elasticity; ε_{fu} = ultimate tensile strain of FRP; n_{slb} = the number of steel longitudinal bars; d_{slb} = the diameter of steel longitudinal bars; f_{yl} = the yield stress of steel longitudinal bar; d_{sth} = the diameter of steel transverse reinforcements; s = the distance between steel hoops/spirals; f_{yh} = the yield stress of steel transverse reinforcements; Steel type: hoop (H) and spiral (S).

$$f_{ls,y} = K_{ls}\varepsilon_{yh} = 2k_{vs}\frac{A_{sh}f_{yh}}{D_c s} \tag{20}$$

$$k_{vs} = \left(1 - \frac{s}{2D_c}\right)^2 = (1 - 0.5R_s)^2 \text{ for steel hoops} \tag{21a}$$

$$k_{vs} = 1 - \frac{s}{2D_c} = 1 - 0.5R_s \text{ for steel spirals} \tag{21b}$$

where the "S" in the subscript represents the steel confinement imposed to the concrete core of SCC; $f_{ls,y}$ is the steel confinement pressure corresponding to the yield stress of the steel spiral/hoop; k_{vs} is the reduction factor reflecting the effect of vertical arching action between steel hoops/spirals; D_c is the diameter of the concrete core; A_{sh} is the cross-sectional area of a steel confining spiral/hoop; E_s, ε_{yh} and f_{yh} are the elasticity modulus, yield strain and stress of steel transverse reinforcements, respectively; s is the distance between steel hoops/spirals; $R_s = s/D_c$ is the normalized steel hoop/spiral spacing.

Accordingly, in order to derive a rational formulation for f_{ctr}^{FS}, two extreme conditions should be considered in its establishment: i) for FCRC with a low level of FRP confinement ($K_{Lf} \simeq 0$), where f_{ctr}^{FS} should approach f_{cc}^{S}, representing that improvements generated by FRP-steel confinement is equal to steel confinement-induced ones; ii) when the steel confinement stiffness of FCRC is very insignificant ($K_{Ls}/K_{Lf} \simeq 0$), f_{ctr}^{FS} can be assumed reasonably identical to f_{ctr}^{F}, representing that FRP confinement controls FCRC's behavior. According to these considerations, a new formulation was developed for the calculation of f_{ctr}^{FS} as follows:

$$\frac{f_{ctr}^{FS}}{f_{ctr}^{F}} = 1 + \frac{\Delta_{f,s}}{1 + \eta_f} \tag{22}$$

where $\eta_f \geqslant 0$ is the calibration term. For the case of $K_{Lf} \simeq 0$ ($f_{ctr}^{F} \simeq f_{c0}$ based on Eq. (14)), η_f should be almost zero for a reliable transformation of Eq. (22) from FCRC to SCC. Moreover, since $\Delta_{f,s}$ is almost null for a low level of steel confinement stiffness ($K_{ls} \simeq 0$ and, subsequently, $f_{ls,y} \simeq 0$), f_{ctr}^{FS} would be virtually the same of f_{ctr}^{F}. Taking into the account these considerations, the following equation is obtained from the best-fit relationship between η_f and key variables through regression analysis performed on 51 test data of FCRC collected in the database, as:

$$\eta_f = 5 \times 10^{-5}\frac{K_{Lf}^{0.06} f_{yh}^{2.5} R_D^{1.3}}{\lambda_s \lambda_K f_{c0}^{1.4} R_s^{0.58}(1 + 14c/D)} \tag{23}$$

in which

$$\lambda_K = 12 + 0.02K_{Lf} \tag{24}$$

where $\lambda_f = 1.55$ and $\lambda_f = 1$ for steel hoops and spirals, respectively. R_D is the normalized column dimension, as $R_b = D/150$. c is the thickness of the concrete cover. In Fig. 4, the performance of the proposed predictive model for the transition strength is assessed. As can be seen, by using η_f from Eq. (23), the experimental counterparts of f_{ctr}^{FS} could be closely predicted by Eq. (22), confirming their reliability.

In this study, a similar methodology with that developed for the establishment of transition strength is adopted to find a formulation for the transition strain (ε_{ctr}^{FS}). Accordingly, two conditions should be considered in the establishment of a rational formulation for ε_{ctr}^{FS}:

I. ε_{ctr}^{FS} approaches ε_{cc}^{S} by decreasing K_{Lf}, particularly for the case with $K_{Lf}/K_{Ls} \simeq 0$ (representing FCRC with low level of FRP confinement or/and a high level of steel confinement).
II. ε_{ctr}^{FS} approaches ε_{ctr}^{F} by decreasing K_{Ls}, particularly for the case with $K_{Ls}/K_{Lf} \simeq 0$(representing FCRC with high level of FRP confinement or/and a low level of steel confinement).

Based on Mander *et al.* [18]'s recommendation, ε_{cc}^{S} corresponding to f_{cc}^{S} (Eq. (18)) for SCC can be calculated:

$$\frac{\varepsilon_{cc}^{S}}{\varepsilon_{c0}} = 1 + 5\left[\frac{f_{cc}^{S}}{f_{c0}} - 1\right] \tag{25}$$

Replacing Eq. (18) into Eq. (25) leads to

$$\frac{\varepsilon_{cc}^{S}}{\varepsilon_{c0}} = 1 + 5\Delta_{f,s} \tag{26}$$

By considering the aforementioned conditions (I and II), to satisfy the condition II as well as I, a new formulation was developed for the calculation of ε_{ctr}^{FS} as follows:

$$\frac{\varepsilon_{ctr}^{FS}}{\varepsilon_{ctr}^{F}} = 1 + 5\frac{\Delta_{f,s}}{1 + \eta_\varepsilon} \tag{27}$$

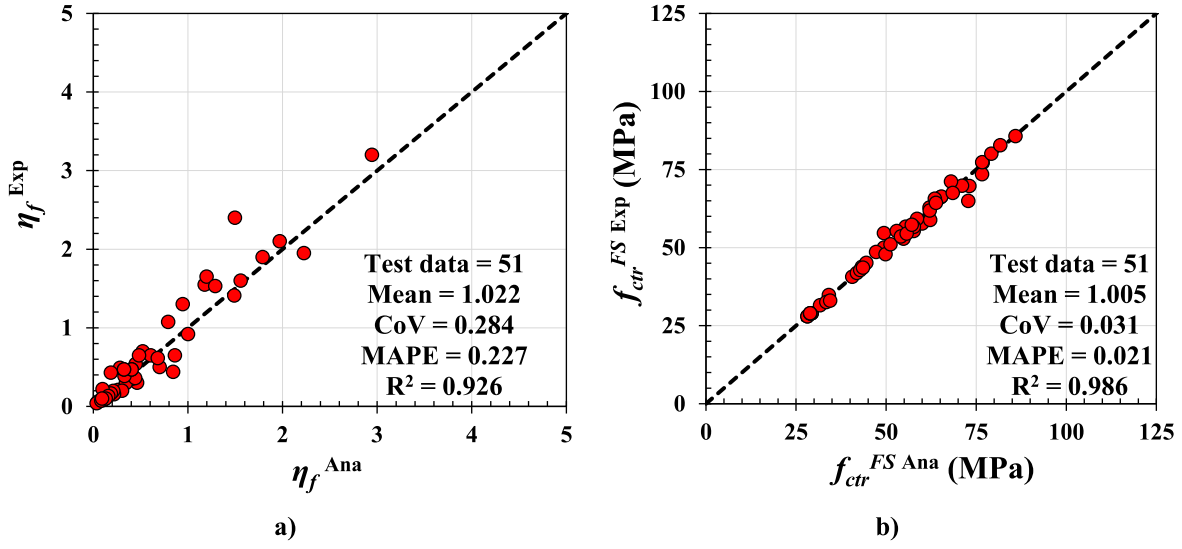

Fig. 4. Performance of: a) Eq. (22) and, b) Eq. (23).

where $\eta_\varepsilon \geqslant 0$ is the calibration term. For FCRC with $K_{Lf} \simeq 0$ ($\varepsilon^F_{ctr} \simeq \varepsilon_{c0}$), η_ε should be almost zero for extending the application of Eq. (27) not only to FCRC, but also to SCC. Taking into the account this consideration, the following equation was obtained from the best-fit relationship between η_ε and key variables through regression analysis performed on 75 test data of FCRC collected in the database:

$$\eta_\varepsilon = \frac{0.44 f_{c0}^{1.8} R_D^{0.97} K_{Lf}^{0.22}}{\lambda_\varepsilon R_s^{0.18} f_{yh}^{0.75}} \tag{28}$$

where $\lambda_\varepsilon = 2$ and $\lambda_\varepsilon = 1$ for steel hoops and spirals, respectively. Fig. 5 shows that by obtaining η_ε from Eq. (28), Eq. (27) could provide a good performance in the prediction of the experimental counterparts of ε^{FS}_{ctr}.

6. Determination of E_2^{FS}

A new formulation is proposed for the calculation of the slope of the second branch of the stress–strain relationship (E_2^{FS}) of FCRC. To develop a reliable formulation for E_2^{FS}, it should have a unified character with E_2^F of FCC with $K_{ls} = 0$. Therefore, once E_2^F is available, beneficial influence of steel transverse reinforcements on the second branch of FCRC's axial behavior can be evaluated, and considered subsequently in the establishment of the formulation of E_2^{FS}.

Based on the model developed by Lam and Teng [40] for E_2^F of FCC (which can be adopted for concrete cover), it can be given as:

$$E_2^F = \frac{f^F_{cu} - f_{c0}}{\varepsilon^F_{cu}} \tag{29}$$

where f^F_{cu} and ε^F_{cu} are the ultimate axial strength and its corresponding ultimate axial strain at FRP rupture strain ($\varepsilon_{h,rup}$). Considering that the FRP confinement-induced improvement in terms of f^F_{cu} is dependent on FRP lateral pressure ($f^F_{l,rup} = K_{Lf}\varepsilon_{h,rup}$) at the rupture of FRP jacket, f^F_{cu} can be expressed as:

$$f^F_{cu} = f_{c0} + \beta_1 K_{Lf}\varepsilon_{h,rup} \tag{30}$$

where β_1 is the calibration factor of this equation. On the other hand, based on secant Poisson's ratio effect (lateral-to-axial strain ratio), ε^F_{cu} as an input parameter in Eq. (29) can be derived as the ratio of $\varepsilon_{h,rup}$ to ultimate secant Poisson's ratio (υ_u), leading to $\varepsilon^F_{cu} = \varepsilon_{h,rup}/\upsilon_u$. Studies ([4,41–43]) evidenced that υ_u is mainly dependent on K_L and f_{c0} ($\upsilon_u = g[K_L, f_{c0}]$). Consequently, a regression-based structure for ε^F_{cu} can be given by:

$$\varepsilon^F_{cu} = \frac{\varepsilon_{h,rup}}{\upsilon_u} \simeq \beta_2 K_{Lf}^{\beta_3} f_{c0}^{\beta_4} \varepsilon_{h,rup} \tag{31}$$

where β_2 to β_4 are the calibration factors. Thus, introducing Eqs. (30) and (31) into Eq. (29) yields:

$$E_2^F = \frac{f^F_{cu} - f_{c0}}{\varepsilon^F_{cu}} = \frac{\beta_1}{\beta_2} K_{Lf}^{1-\beta_3} f_{c0}^{-\beta_4} \tag{32}$$

Note that it is possible to determine the calibration factors of β_1 to β_4 by performing a regression analysis on experimental data of f^F_{cu} and ε^F_{cu} [40]. Nonetheless, due to the structure of Eq. (32), there is a great opportunity to calibrate the equation directly from experimental data of E_2^F. Hence, Eq. (32) was rearranged as:

$$E_2^F = \beta_5 K_{Lf}^{\beta_6} f_{c0}^{\beta_7} \tag{33}$$

where β_5 to β_7 are the calibration factors, which are required to be determined directly from experimental values of E_2^F. For this purpose, a large database was collected from the slope of the final segment of stress–strain experimental curves of FCC. Based on regression analysis implemented on 583 test data of E_2^F, Eq. (33) was calibrated as follows:

$$E_2^F = 3.38\gamma_{fc} E_f^{0.15} K_{Lf}^{0.47} f_{c0}^{0.31} \tag{34}$$

in which

$$0.8 \leqslant \gamma_{fc} = \frac{f_{c0}}{25} \leqslant 1 \tag{35}$$

whose suitable predictive performance is shown in Fig. 6a.

Considering the fact that E_2^{FS} is much dependent on FRP confinement rather than on steel confinement (Lin *et al.* [24]), in this study, the beneficial effect of steel transverse reinforcements on E_2^{FS} was simulated based on the formulation developed exclusively for FCC. Accordingly, E_2^{FS} can be given by:

$$E_2^{FS} = \eta_E E_2^F \tag{36}$$

where η_E is the calibration factor to adjust the effect of K_{Ls} on E_2^{FS}. Using regression analysis technique on 75 test data representing the slope of the final branch of experimental stress–strain curves of FCRC, the following equation was developed to estimate η_E:

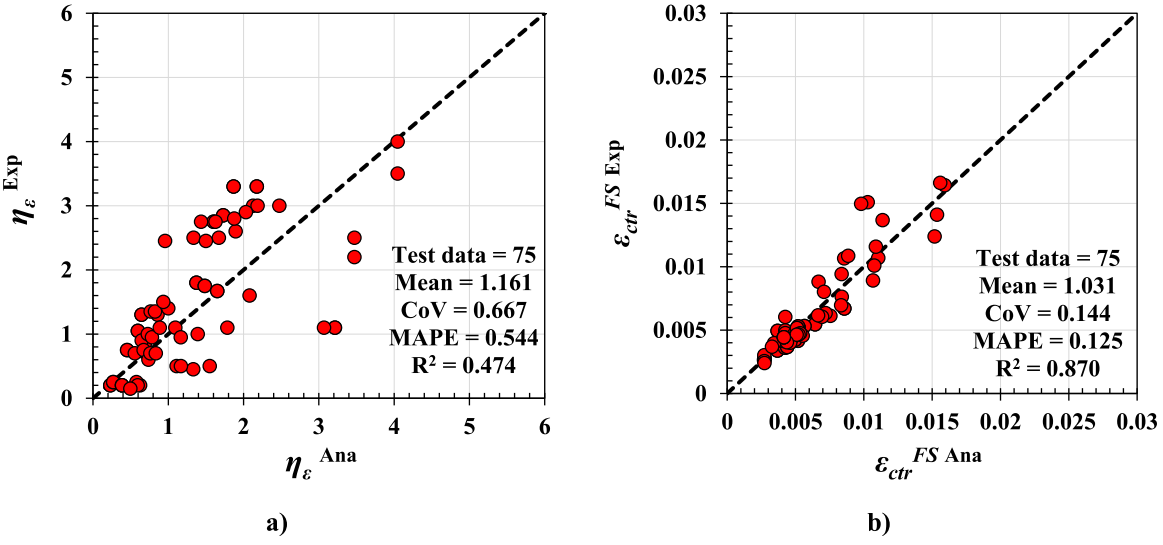

Fig. 5. Predictive performance of Eqs. (27) and (28).

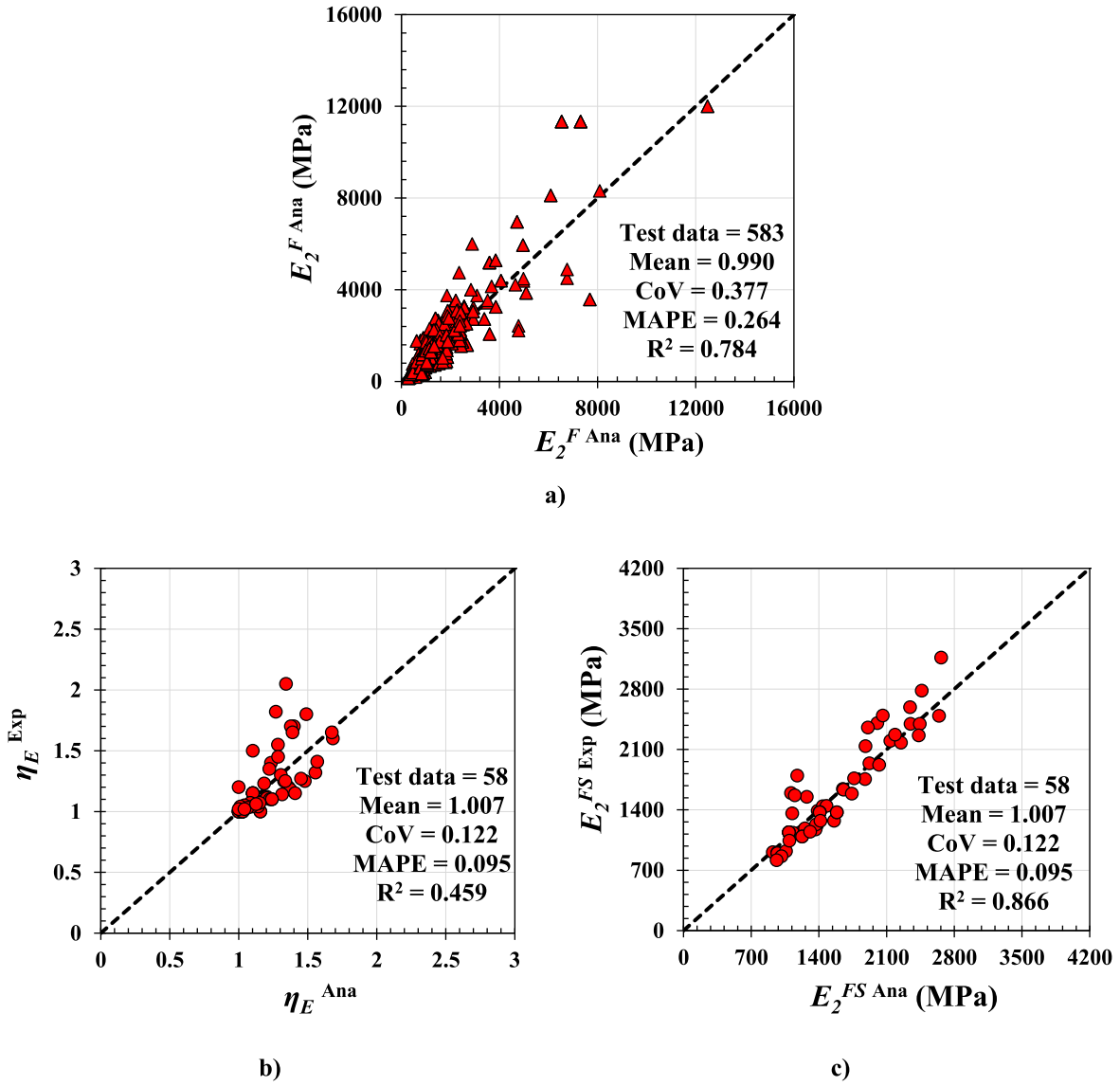

Fig. 6. Predictive performance of a) Eq. (34), b) Eq. (37) and c. Eq. (36).

$$\eta_E = 1.7\frac{K_{Ls}^{0.1} f_{c0}^{0.08}}{\lambda_E K_{Lf}^{0.1} f_{yh}^{0.1}(1.15 - 1.85c/D)} \tag{37}$$

where $\lambda_E = 0.47$ and $\lambda_E = 1$ for steel hoops and spirals, respectively. K_{ls} is the lateral confinement stiffness due to steel hoops ($= 2k_{vs}\frac{A_{sh}E_{sh}}{D_c s}$). Fig. 6b and 6c show that by obtaining the model parameter of η_E from Eq. (37), the experimental counterparts of E_2^{FS} could be predicted by Eq. (36) with adequate accuracy.

7. Determination of n_d

The stress–strain gradient of the first branch of the axial stress–strain curve, defined by the n_d parameter in Eqs. (4) and (8), was obtained based on regression-based formulation by considering experimental observations, as follows:

$$n_d = n_{d0}\psi_f\psi_s > 1 \tag{38}$$

where n_{d0} is the term of the exponent representing the shape of the first parabolic portion of unconfined concrete's axial behavior; ψ_f and ψ_s are the term considered to reflect the influences of FRP and steel confinement systems on n_d.

For obtaining n_{d0}, a test database of unconfined concrete columns, in which $\psi_f = 1$ and $\psi_s = 1$, was collected. For this purpose, n_{d0}^{Exp} was determined by applying Eq. (38) on pre-peak stress–strain relationship of 85 experimental specimens, so that Eq. (11) could estimate the counterparts' response, with adequate accuracy. In the case of unconfined concrete columns, $f_{ctr}^F = f_{c0}$, $\varepsilon_{ctr}^F = \varepsilon_{c0}$, and $E_{ctr}^F = 0$ were considered. Performing statistical analysis, a new formulation was developed based on the best-fit relation of n_{d0}^{Exp} with key variables, i.e. f_{c0}, L/D and D, as follows:

$$n_{d0} = \frac{0.77 f_{c0}^{0.4}(L/D)^{0.1}}{1 + D/300} \tag{39}$$

whose predictive performance can be seen in Fig. 7a.

For obtaining ψ_f, a test database of FCC ($\psi_s = 1$), including 178 data of ψ_f^{Exp}, was collected. By implementing Eq. (38), using n_{d0} obtained from Eq. (39), in the first-segment of axial stress–strain curve of FCC, ψ_f^{Exp} was derived so that the analytical response could coincide accurately with the counterparts' response. Based on regression analysis technique, the following expression was developed:

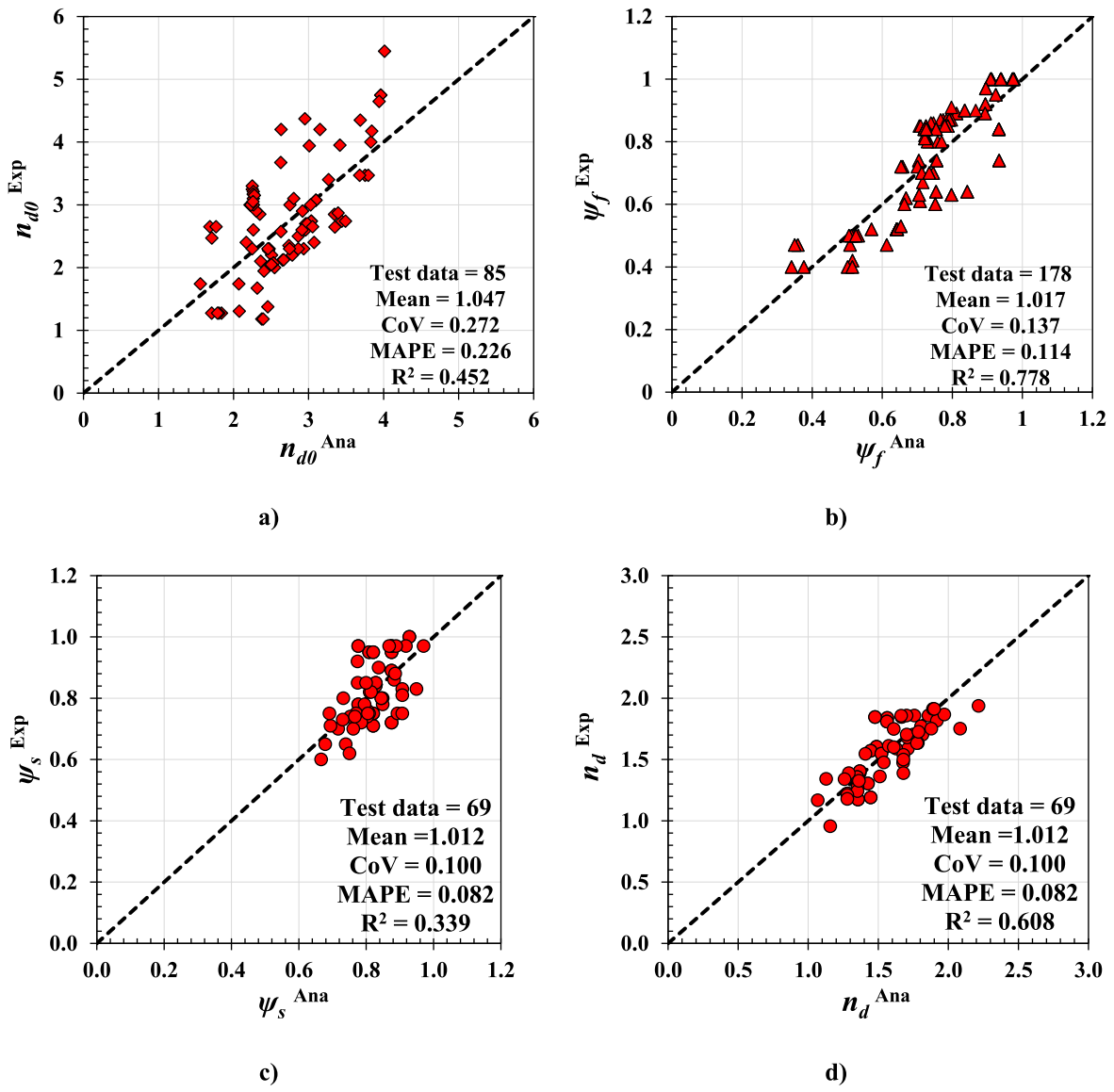

Fig. 7. Predictive performance of Eqs. (39), (40), (41) and (38).

$$\psi_f = 1 - K_L^{0.02}(0.0032 f_{c0} - 0.1) \leqslant 1 \tag{40}$$

whose predictive performance can be seen in Fig. 7b.

Similarly, for developing a formulation for ψ_s, a test database of FCRC, including 69 data of ψ_s^{Exp}, was collected. By implementing Eq. (38), using n_{d0} and ψ_f obtained from Eqs. (39) and (40), in the first branch of the axial stress–strain curve of FCRC, ψ_s^{Exp} was obtained so that Eq. (38) could estimate the counterparts' response, with adequate accuracy. Based on regression analysis technique, the following expression was derived for ψ_s:

$$\psi_s = 1.6 R_s^{0.15} K_L^{-0.08} \leqslant 1 \tag{41}$$

whose predictive performance can be seen in Fig. 7c. Fig. 7d shows that Eq. (38) to estimates the exponent of the polynomial functions (n_d) with good agreement between the predictions and experimental counterparts of n_d.

8. Calculation process

The procedure of the developed model for the calculation of the load-carrying capacity (N) versus axial strain (ε_c) relationship of FCRC under axial compressive loading comprises the following three main steps (Fig. 8):

For concrete cover:

i. Determine the transition stress (f_{ctr}^F) using Eq. (14).
ii. Determine the transition strain (ε_{ctr}^F) using Eq. (15).
iii. Determine the slope of the second branch (E_2^F) using Eq. (34).
iv. Calculate the axial stress–strain relationship (f_c^{Cover} *vs* ε_c) using Eq. (4).

For concrete core:

v. Determine the model parameters of η_f, η_ε, η_E and n_d by using Eqs. (23), 28, 37 and 38).
vi. Determine the transition stress (f_{ctr}^{FS}) using Eq. (22).

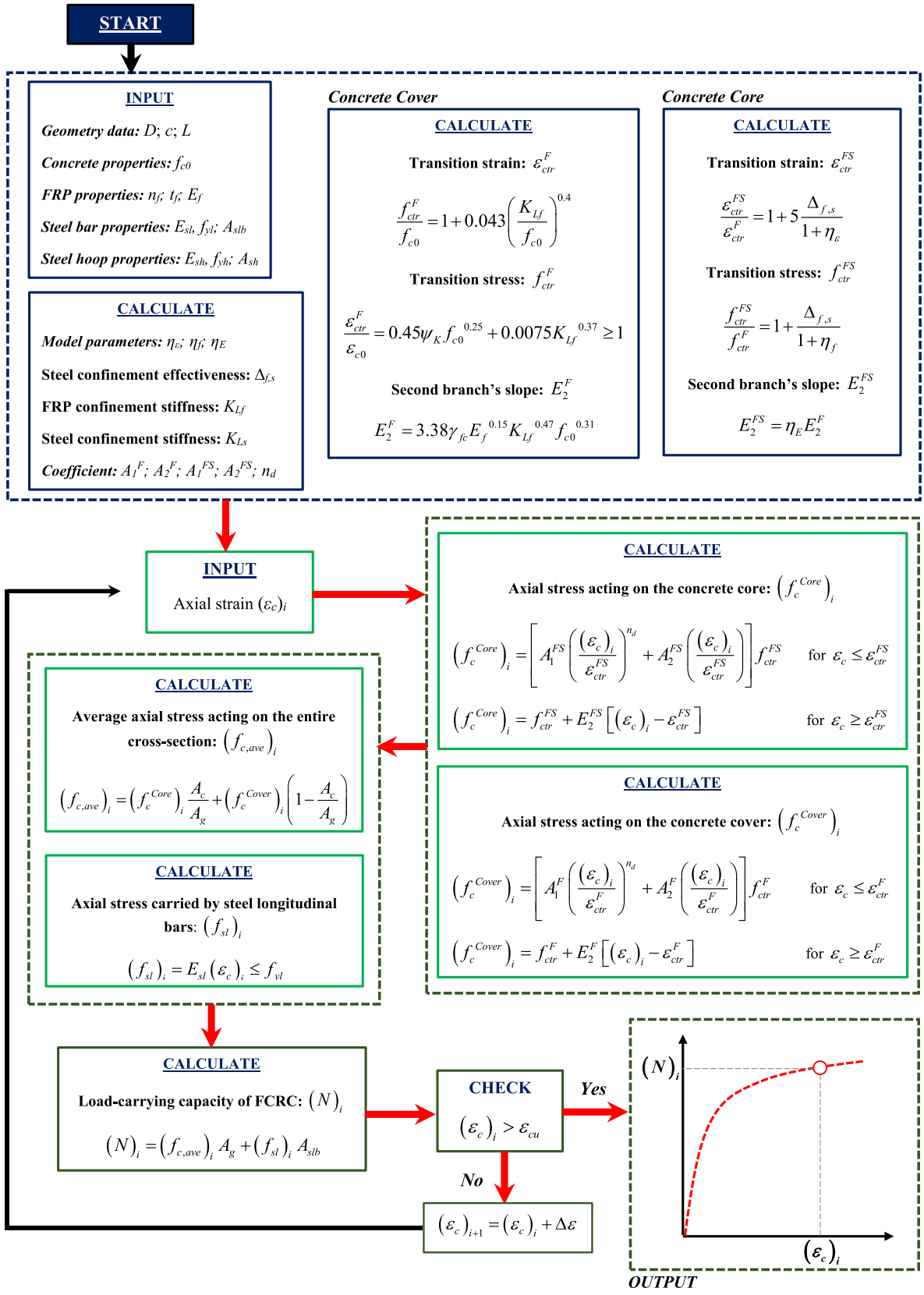

Fig. 8. A flowchart for determining load-carrying capacity versus axial strain relation of FCRC.

vii. Determine the transition strain (ε_{cr}^{FS}) using Eq. (27).
viii. Determine the slope of the second branch (E_2^{FS}) using Eq. (36).
ix. Calculate the axial stress–strain relation (f_c^{Core} *vs* ε_c) using Eq. (8).

For steel longitudinal bar:

x. Calculate the axial stress–strain relation (f_{sl} *vs* ε_c) using Eq. (3)

For the entire cross-section of FCRC:

xi. Calculate load-carrying capacity versus strain relation of FCRC (N *vs* ε_c) using Eq. (1)

Note that since the main focus of the developed model is the prediction of the full load-carrying capacity versus strain response of FCRC, the experimental value of ultimate axial strain is used for terminating the calculation process. A predictive formulation to determine the ultimate condition of FCRC will be the subject of a future research study.

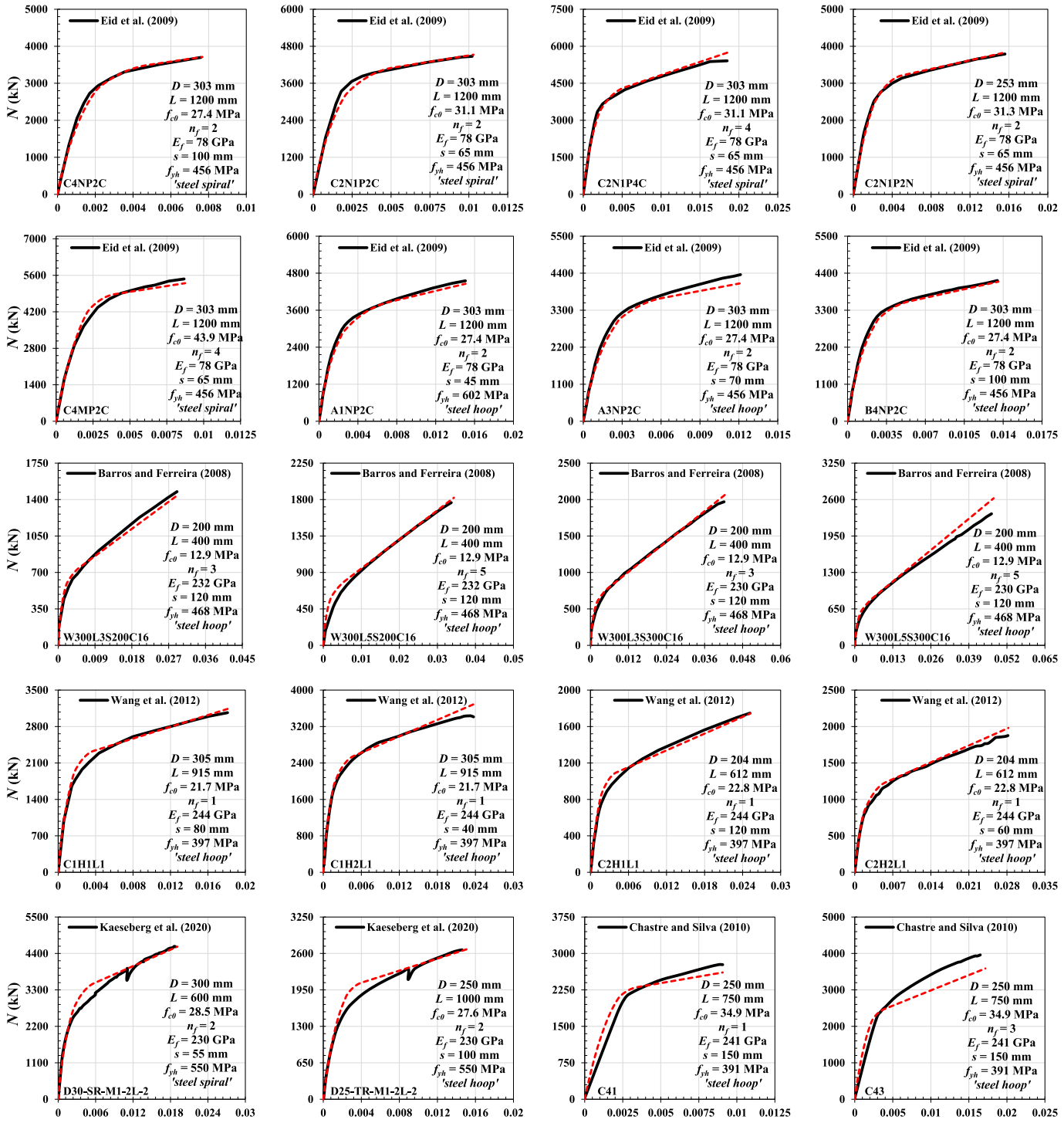

Fig. 9. Analytical predictions versus experimental stress–strain responses of FCRC reported by: Demers and Neale [30], Pessiki et al. [31], Matthys et al. [32], Barros and Ferreira [3], Eid et al. [5], Lee et al. [8], Chastre and Silva [33], Wang et al. [2], Zhang [34], Wei et al. [7,35] and Kaeseberg et al. [6].

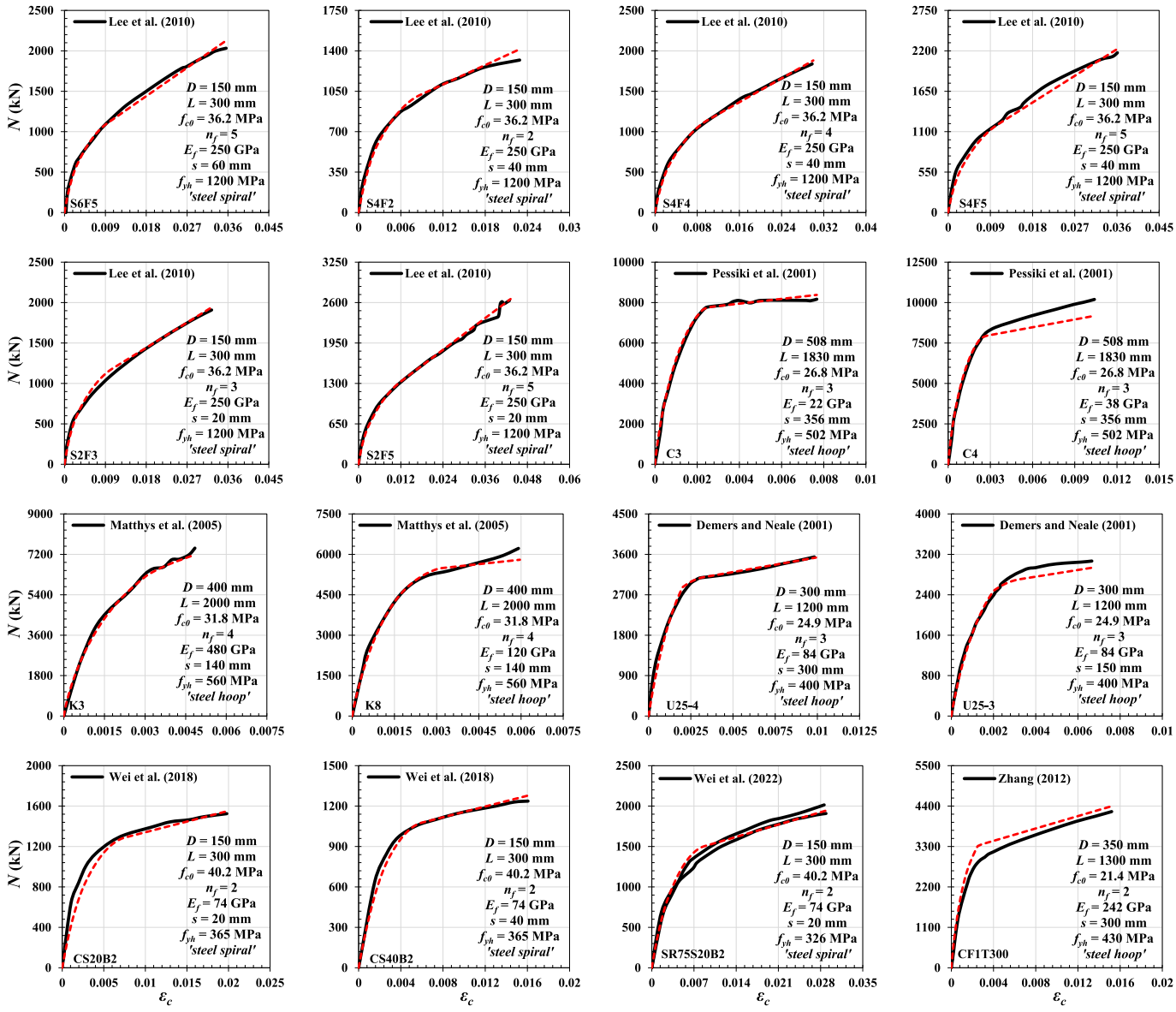

Fig. 9. (*continued*).

9. Comparison with experimental load-carrying capacity vs axial strain relation

The reliability of the developed model is not only a function of the accuracy of its key coordinates, but also dependent on its performance in simulating full load-carrying capacity versus axial strain relation with sufficient precision. This section accesses the performance of the proposed model in terms of predicting the axial response of FCRC under compressive loading. Hence, the load-carrying capacity versus axial strain obtained from the proposed model is compared with those data of FCRC registered experimentally in the literature. Additionally, the proposed model's performance is compared with that of existing models conducted by Wang *et al.* [2], Hu and Seracino [16], Teng *et al.* [1], Lin *et al.* [24], ACI440.2R-17 [25] and *fib* [26]. These models can be categorized into two groups of AOM (Hu and Seracino [16], Teng *et al.* [1]) and DOM (Wang *et al.* [2], Lin *et al.* [24], ACI440.2R-17 [25] and *fib* [26]). Among these models, ACI440.2R-17 [25] and *fib* [26] were founded on Lam and Teng [40]'s DOM developed exclusively for FCC, where the effect of internal steel hoop/spiral reinforcements on load-carrying capacity of FCRC was ignored. The model developed by Wang et al. [2] considered an average level of axial stress–strain responses for both concrete cover and core regions by ignoring their difference, whereas Hu and Seracino [16], Teng *et al.* [1], Lin *et al.* [24] models provided separate behavior for these regions.

In Fig. 9, the load-carrying capacity versus axial strain responses of FCRC predicted analytically by the proposed model are compared with those experimentally conducted by Demers and Neale [30], Pessiki *et al.* [31], Matthys *et al.* [32], Barros and Ferreira [3], Eid *et al.* [5], Lee *et al.* [8], Chastre and Silva [33], Wang *et al.* [2], Zhang [34], Wei *et al.* [7,35] and Kaeseberg *et al.* [6]. As can be observed, the proposed model is able to provide a suitable predictive performance for the axial behavior of the experimental counterparts having various levels of geometry, material and FRP-steel confinement properties.

In Fig. 10, the comparative assessment of the developed model with the other existing ones is presented. As expected, ACI440.2R-17 [25], and *fib* [26] underestimated the response of FCRC columns due to the ignorance of internal steel confining reinforcements. For some cases, misleading results were achieved by the model suggested by Wang *et al.* [2]. The models developed by Hu and Seracino [16] and Teng *et al.* [1] led to conservative predictions of the experimental counterparts. In

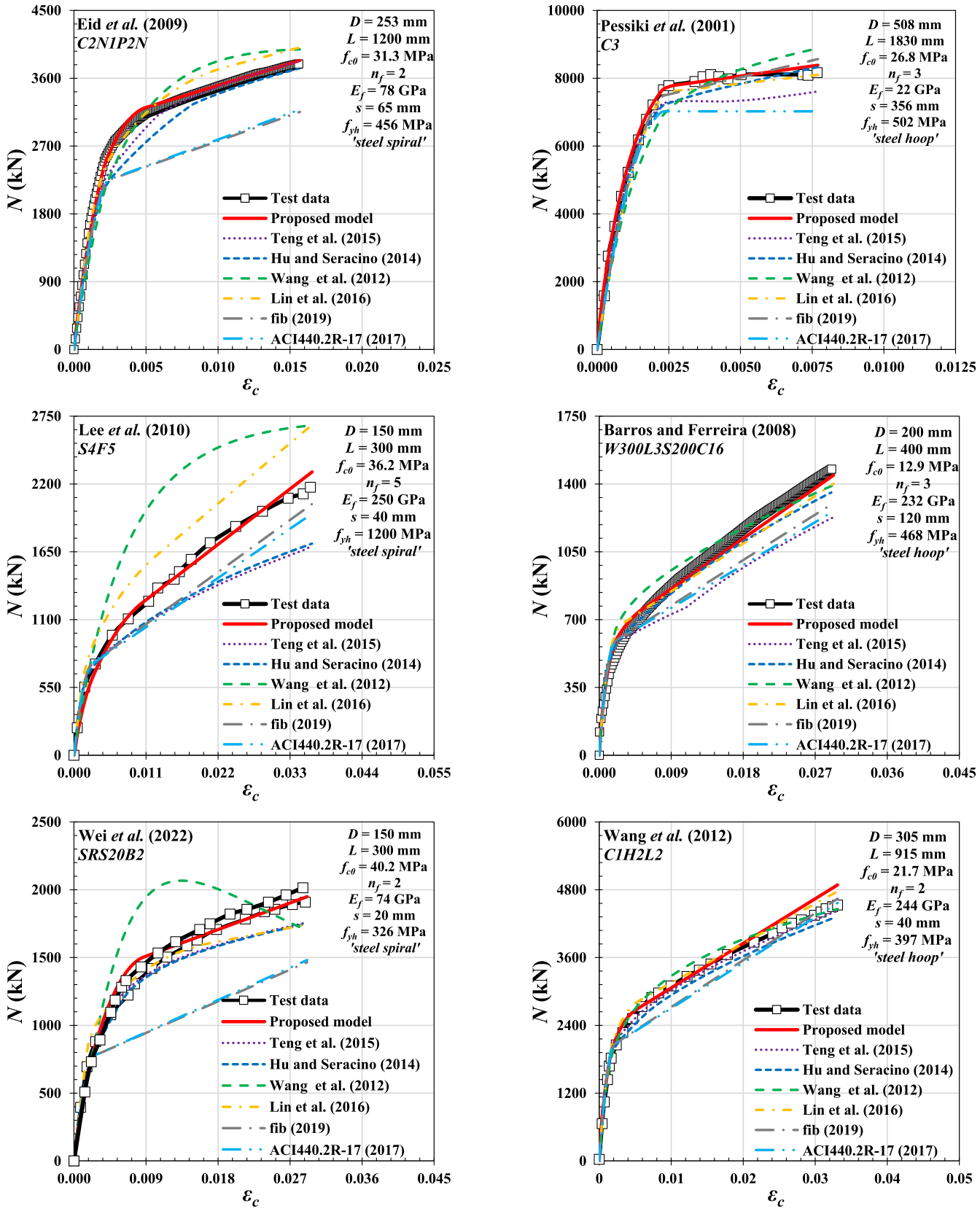

Fig. 10. Analytical predictions versus experimental stress–strain responses of FCRC reported by: Pessiki et al. [31], Barros and Ferreira [3], Eid et al. [5], Lee et al. [8], Wang et al. [2], and Wei et al. [35].

general, Lin *et al.* [24]'s model demonstrated the best performance among the existing models. Nonetheless, it can be seen from Fig. 9, the proposed model provides a superior performance compared to the other ones, in the prediction of the experimental load-carrying capacity versus axial strain behavior of the FCRC columns.

Since a relatively simple methodology was developed in the present study, the proposed model, exclusively established for circular cross-section columns confined by FRP jacket, can be potentially extended for FRP-confined non-circular (square and rectangular) cross-section concrete columns under axial compressive loading. For this purpose, the effect of non-circularity on the second branch's slopes (E_2^F and E_2^{FS}, presented by Eqs. (34) and (36)) of the stress–strain relations for concrete cover and core should be formulated by developing reduction factors comprising corner radius ratio ($R_b = 2r/b$ where$b$ = shorter side of the section and$r$ = corner radius length) and cross-sectional aspect ratio ($R_\lambda = h/b$ where$h$ = longer side of the section) [44]. The non-circularity effect should be also reflected in the transition zone-related information (f_{ctr}^{FS}, ε_{ctr}^{FS},f_{ctr}^{F}, and ε_{ctr}^{F}, presented by Eqs. (22), (27), (14) and (15)). Furthermore, the model parameters of η_f, η_ε, η_E and n_d should be updated so that load-carrying capacity versus axial strain relationship of FCRC could be precisely estimated through the proposed stress–strain model, which will be explored in future research studies.

10. Summary and conclusion

In this paper, a new design-oriented stress–strain model for FRP-confined RC columns (FCRC) under axial compressive loading was proposed. In this model, the cover concrete region (subjected to only FRP confinement) and the core concrete zone (subjected to a combined FRP-steel confinement) were treated separately. The proposed model, consisting of parabolic and linear segments, was established based on the key states and complete load-carrying capacity versus axial strain relation of FCRC as shown by experimental results. The stress–strain gradient of the first branch (n_d) was adjusted by developing a new regression-based formulation by considering a series of experimental data of unconfined concrete, FRP-confined concrete columns (FCC) and FCRC. New formulations with sufficient accuracy were developed to determine transition zone-related information (f_{ctr}^{FS} and ε_{ctr}^{FS}) with statistical indicators demonstrating the high predictive performance, namely Mean = 1.005, CoV = 0.031, MAPE = 0.021 and R^2 = 0.986, and Mean = 1.031, CoV = 0.144, MAPE = 0.125 and R^2 = 0.870, respectively. A new methodology was proposed to develop a new expression for the second branch's slope of axial response of FCC (E_2^F). This expression was extended for FCRC by reflecting the significant influence of dual FRP-steel confinement in the second branch's slope (E_2^{FS}) through regression analysis with the obtained statistical indicators as Mean = 1.007, CoV = 0.122, MAPE = 0.095 and R^2 = 0.866. By comparing with many test results, the suitable predictive performance of the proposed stress–strain model in the close prediction of experimental load-carrying capacity versus axial strain relation of FCRC subjected to compression was demonstrated. Based on the results obtained from the comparative study, even though it was found that Lin *et al.* [24]'s model could show the best performance among the existing models, the proposed model provided superior predictive performance.

It is worth noting that even though the model proposed in this study provides a good balance between the simplicity of the implementation and the accuracy of simulation, it cannot be considered a ready-made solution for the direct application in practical design, where safety factors are required to be determined on the basis of reliability analysis concept. Furthermore, the extension of the proposed model for the cases of FRP-confined square/rectangular RC columns and eccentrically loaded FRP-confined RC columns will be explored in future research studies.

CRediT authorship contribution statement

Javad Shayanfar: Conceptualization, Data curation, Methodology, Validation, Writing – original draft. **Joaquim A.O. Barros:** Conceptualization, Methodology, Supervision, Writing – review & editing. **Mohammadali Rezazadeh:** Conceptualization, Methodology, Supervision, Writing – review & editing.

Declaration of competing interest

The authors declare that they have no known competing financial interests or personal relationships that could have appeared to influence the work reported in this paper.

Data availability

Data will be made available on request.

Acknowledgments

This study is a part of the project ''Sticker –Innovative technique for the structural strengthening based on using CFRP laminates with multifunctional attributes and applied with advanced cement adhesives'', with the reference POCI-01-0247-FEDER-039755. This work was partly financed by FCT / MCTES through national funds (PIDDAC) under the R&D Unit Institute for Sustainability and Innovation in Structural Engineering (ISISE), Portugal under reference UIDB/04029/2020, and under the Associate Laboratory Advanced Production and Intelligent Systems ARISE, Portugal under reference LA/P/0112/2020. The first author also acknowledges the support provided by FCT, Portugal PhD individual fellowship 2019 with the reference of "SFRH/BD/148002/2019".

References

[1] Teng JG, Lin G, Yu T. Analysis-oriented stress-strain model for concrete under combined FRP-steel confinement. J Compos Constr 2015;19(5):04014084.
[2] Wang Z, Wang D, Smith ST, Lu D. Experimental testing and analytical modeling of CFRP-confined large circular RC columns subjected to cyclic axial compression. Eng Struct 2012;40:64–74.
[3] Barros JA, Ferreira DR. Assessing the efficiency of CFRP discrete confinement systems for concrete cylinders. J Compos Constr 2008;12(2):134–48.
[4] Shayanfar J, Rezazadeh M, Barros JA. Analytical model to predict dilation behavior of FRP confined circular concrete columns subjected to axial compressive loading. J Compos Constr 2020;24(6):04020071.
[5] Eid R, Roy N, Paultre P. Normal- and high-strength concrete circular elements wrapped with FRP composites. J Compos Constr 2009;13(2):113–24.
[6] Kaeseberg S, Messerer D, Holschemacher K. Experimental study on concrete under combined FRP–Steel confinement. Materials 2020;13(20):4467.
[7] Wei Y, Zhang X, Wu G, Zhou Y. Behaviour of concrete confined by both steel spirals and fiber-reinforced polymer under axial load. Compos Struct 2018;192:577–91.
[8] Lee JY, Yi CK, Jeong HS, Kim SW, Kim JK. Compressive response of concrete confined with steel spirals and FRP composites. J Compos Mater 2010;44(4):481–504.
[9] Yin P, Huang L, Yan L, Zhu D. Compressive behavior of concrete confined by CFRP and transverse spiral reinforcement. Part A: experimental study. Mater Struct 2016;49:1001–11.
[10] Benzaid R, Mesbah H, Chikh NE. FRP-confined concrete cylinders: axial compression experiments and strength model. J Reinf Plast Compos 2010;29(16):2469–88.
[11] Issa MA, Alrousan RZ, Issa MA. Experimental and parametric study of circular short columns confined with CFRP composites. J Compos Constr 2009;13(2):135–47.
[12] Zignago D, Barbato M. Effects of transverse steel on the axial-compression strength of FRP-confined reinforced concrete columns based on a numerical parametric study. J Compos Constr 2021;25(4):04021024.
[13] Carey SA, Harries KA. Axial behavior and modeling of confined small-, medium-, and large-scale circular sections with carbon fiber-reinforced polymer jackets. ACI Struct J 2005;102(4):596.
[14] Ilki A, Peker O, Karamuk E, Demir C, Kumbasar N. FRP retrofit of low and medium strength circular and rectangular reinforced concrete columns. J Mater Civ Eng 2008;20(2):169–88.
[15] Bai YL, Dai JG, Teng JG. Buckling of steel reinforcing bars in FRP-confined RC columns: An experimental study. Constr Build Mater 2017;140:403–15.
[16] Hu H, Seracino R. Analytical model for FRP-and-steel-confined circular concrete columns in compression. J Compos Constr 2014;18(3):A4013012.

[17] Jiang T, Teng JG. Analysis-oriented stress–strain models for FRP–confined concrete. Eng Struct 2007;29(11):2968–86.
[18] Mander JB, Priestley MJ, Park R. Theoretical stress-strain model for confined concrete. J Struct Eng 1988;114(8):1804–26.
[19] Shayanfar J, Barros JA, Rezazadeh M. Analysis-oriented model for partially FRP-and-steel-confined circular RC columns under compression. Eng Struct 2023;276:115330.
[20] Shayanfar J, Barros JA, Rezazadeh M. Unified model for fully and partially FRP confined circular and square concrete columns subjected to axial compression. Eng Struct 2022;251:113355.
[21] Eid R, Paultre P. Analytical model for FRP-confined circular reinforced concrete columns. J Compos Constr 2008;12(5):541–52.
[22] Légeron F, Paultre P. Uniaxial confinement model for normal-and high-strength concrete columns. J Struct Eng 2003;129(2):241–52.
[23] Pellegrino C, Modena C. Analytical model for FRP confinement of concrete columns with and without internal steel reinforcement. J Compos Constr 2010;14(6):693–705.
[24] Lin G, Yu T, Teng JG. Design-oriented stress–strain model for concrete under combined FRP-steel confinement. J Compos Constr 2016;20(4):04015084.
[25] ACI 440.2R-17. Guide for the design and construction of externally bonded FRP systems for strengthening concrete structures; American Concrete Institute (ACI): Farmington Hills MI USA 2017.
[26] Fib Bulletin 90. Externally applied FRP reinforcement for concrete structures. Task Group 5. 1, International Federation for Structural Concrete 2019.
[27] Shayanfar J, Omidalizadeh M, Nematzadeh M. Analysis-oriented model for seismic assessment of RC jacket retrofitted columns. Steel Compos Struct Int J 2020;37(3):371–90.
[28] Shayanfar J, Bengar HA. A practical model for simulating nonlinear behaviour of FRP strengthened RC beam-column joints. Steel and Composite Struct Int J 2018;27(1):49–74.
[29] Shayanfar J, Akbarzadeh Bengar H. Nonlinear analysis of RC frames considering shear behaviour of members under varying axial load. Bull Earthq Eng 2017;15:2055–78.
[30] Demers M, Neale KW. Confinement of reinforced concrete columns with fibre-reinforced composite sheets-an experimental study. Can J Civ Eng 1999;26(2):226–41.
[31] Pessiki S, Harries KA, Kestner JT, Sause R, Ricles JM. Axial behavior of reinforced concrete columns confined with FRP jackets. J Compos Constr 2001;5(4):237–45.
[32] Matthys S, Toutanji H, Audenaert K, Taerwe L. Axial load behavior of large-scale columns confined with fiber-reinforced polymer composites. ACI Struct J 2005;102(2):258.
[33] Chastre C, Silva MA. Monotonic axial behavior and modelling of RC circular columns confined with CFRP. Eng Struct 2010;32(8):2268–77.
[34] Zhang, Y. X. (2012). "Behavior of large-size FRP-jacketed circular and rectangular reinforced concrete columns." M.Sc. thesis, Dept. of Civil and Environmental Engineering, Hong Kong Polytechnic Univ., Hong Kong.
[35] Wei Y, Xu Y, Wang G, Cheng X, Li G. Influence of the cross-sectional shape and corner radius on the compressive behaviour of concrete columns confined by FRP and stirrups. Polymers 2022;14(2):341.
[36] Sim JI, Yang KH, Kim HY, Choi BJ. Size and shape effects on compressive strength of lightweight concrete. Constr Build Mater 2013;38:854–64.
[37] Shayanfar J, Barros JA, Rezazadeh M. Stress–strain model for FRP confined heat-damaged concrete columns. Fire Saf J 2023;136:103748.
[38] Shayanfar J, Barros JA, Rezazadeh M. Stress-strain model for FRP-confined circular concrete columns developing structural softening behavior. J Compos Constr 2024;28(1):04023065.
[39] Shayanfar J, Barros JA, Rezazadeh M. Analytical model to predict axial stress-strain behavior of heat-damaged unreinforced concrete columns wrapped by FRP jacket. Eng Struct 2023;289:116244.
[40] Lam L, Teng JG. Design-oriented stress–strain model for FRP-confined concrete. Constr Build Mater 2003;17(6–7):471–89.
[41] Shayanfar J, Barros JA, Rezazadeh M. Generalized Analysis-oriented model of FRP confined concrete circular columns. Compos Struct 2021;270:114026.
[42] Jiang K, Han Q, Bai Y, Du X. Data-driven ultimate conditions prediction and stress-strain model for FRP-confined concrete. Compos Struct 2020;242:112094.
[43] Shayanfar, J., Rezazadeh, M., Barros, J., & Ramezansefat, H. (2021). A new dilation model for FRP fully/partially confined concrete column under axial loading. In Proceedings of the 3rd RILEM Spring Convention and Conference (RSCC 2020) Volume 2: New Materials and Structures for Ultra-durability 3 (pp. 435-446). Springer International Publishing.
[44] Shayanfar J, Barros JA, Abedi M, Rezazadeh M. Unified compressive strength and strain ductility models for fully and partially FRP-confined circular, square, and rectangular concrete columns. J Compos Constr 2023;27(6):04023053.